

SPH P³MG Simulations of the Lyman- α Forest

J. W. Wadsley and J. Richard Bond

Canadian Institute for Theoretical Astrophysics and Department of Astronomy, University of Toronto, McLennan Physical Laboratories, Toronto, ONT M5S 1A1, Canada

Abstract. Our understanding of the Lyman- α forest has received a great boost with the advent of the Keck Telescope and large 3D hydrodynamical simulations. We present new simulations using the SPH technique with a P³MG (Particle-Particle Particle-MultiGrid) non-periodic gravity solver. Our method employs a high resolution (1 kpc) inner volume, essential for capturing the complex gas physics, a larger low resolution volume, essential for correct larger scale tidal fields and a self-consistently applied, uniform tidal field to model the influence of ultra long waves. We include a photoionizing UV flux and relevant atomic cooling processes. We use constrained field realisations to probe a selection of environments and construct a statistical sample representative of the wider universe. We generate artificial Lyman- α spectra and fit Voigt profiles. We examine the importance of (1) the photoionizing flux level and history, (2) tidal environment and (3) differing cosmologies, including CDM and CDM+ Λ . With an appropriate choice for the UV flux, we find that the data is fit quite well if the rms density contrast is ~ 1 at $z \sim 3$ on galaxy scales.

To appear in Computational Astrophysics, Proceedings of the 12th Kingston Conference, Halifax, October 1996, ed. D. Clarke & M. West (PASP)

1. Introduction

We hope to be able to use the current wealth of Lyman- α absorption data to constrain the shape and normalisation of the density power spectrum and thus the cosmological model. The extraction of this information is complicated by gas physics, the ultraviolet flux, the star formation history and supernova energy injection. By employing gasdynamical simulations, we can incorporate the detailed high-redshift environment of the clouds self-consistently. We perform our Lyman- α simulations using the SPH method in conjunction with a gravity solver based on the multigrid method. We describe our code, with attention to the novel features, in section 2.

Simulations have to be carefully constructed to achieve both the necessary resolution and simultaneously provide a good sample of the universe. Large scale power is also of particular importance for producing the correct tidal environment for Lyman- α clouds. Recent Lyman- α simulations (*e.g.* Rauch *et al.* (1996), Miralda-Escudé *et al.* (1996), Mücke *et al.* (1996), Davé *et al.* (1996) and Zhang *et al.* (1996)) have traded good k -space resolution $210 - 17.95 \text{ h Mpc}^{-1} \text{ kpc}$ against size, $3 - 22 \text{ Mpc}$. We address these design issues in section 3. and see also Bond & Wadsley (1996), (hereafter BW).

In generating the line statistics of the artificial Lyman- α spectra, it is important to fit the lines in a manner directly comparable with observations (Miralda-Escudé *et al.* (1996), Davé *et al.* (1996)). Our method of fitting Voigt profiles is described with our results in section 4.

2. Numerical Method

Smoothed Particle Hydrodynamics (SPH) is a fully Lagrangian method for fluid dynamics. It has been demonstrated to be robust and flexible (*e.g.* Review by Monaghan (1992)). SPH has the advantage of following collapse of structure with constant mass resolution. Eulerian codes have high gas resolution in voids, but structures arising from small scale perturbations in the early universe are limited to the mass resolution, which is similar in both methods. Eulerian codes without adaptive refinement smooth structure in collapsing regions.

We use a predictor-corrector time stepping scheme allowing us to vary the global timestep. The code runs very quickly at first, but slows when the particle-particle section of the gravity solver becomes dominant.

The code includes radiative cooling and photoionization heating with equilibrium abundances. The species we consider are H, H⁺, He, He⁺, He⁺⁺ and e⁻.

We make use of a highly stable, 2nd order implicit scheme for the energy equation to avoid excessively small timesteps associated with the heating/cooling timescales. We find an iterative solution for the energy, E ,

$$\frac{E(t + \Delta t) - E(t)}{\Delta t} = PdV + (Heat - Cool) \left(T \left(\frac{E(t) + E(t + \Delta t)}{2} \right), \rho \right).$$

The predicted midpoint values for ρ and the PdV work are used.

2.1. The P³MG Gravity Solver

Iterative Full Multigrid techniques provide an excellent alternative to Fourier based PM Methods. Though comparable in speed for a periodic computation, the Multigrid method requires less work for free boundary calculations, by roughly a factor of two. In addition, we take advantage of previous time-step information to increase speed even further by reducing the number of iterations required for convergence. We employ a multipole expansion of the particle potentials to provide boundary conditions for the free boundary calculation. We have added Particle-Particle interactions to dramatically augment the resolution of our gravity solver. The resulting P³MG code achieves $\sim 1\%$ force errors.

For these simulations we have multiple particle masses. We make use of nested grids to optimise our computational costs. We use a 128³ grid with P-P around the high resolution core region with an additional 64³ grid with no P-P forces for the lowest resolution particles whose function is only to provide long range tidal forces. This provides for a maximum resolution of 1 kpc. We set this as the resolution limit for our gas and gravity.

2.2. Enhancements to Standard SPH

SPH relies on weighted sums over near neighbours to estimate all fluid quantities including the pressure forces that move the particles. The method is adaptive, with the smoothing length for the weighted sum being a direct measure of the local resolution.

Appropriately varying smoothing lengths, h , are essential to any SPH implementation. Methods based on numerically estimated quantities such as divergence or density are susceptible to noise whereas what we require is a good sample of neighbouring particles within $2h$. To this end we count neighbours in three equi-volume shells around each

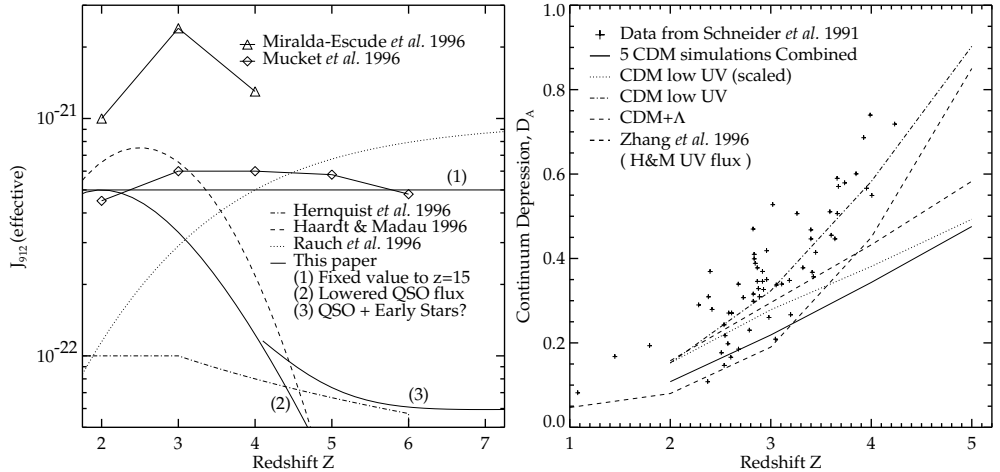


Figure 1. UV Flux history and Continuum Depression, D_A . Curve (2) in the left hand panel was designed to reproduce the D_A vs. redshift data shown in the right panel. A curve such as (3), including an estimate of the UV flux from early stars, is also consistent with the D_A data. The flux model of Haardt & Madau (1996) is too high for standard CDM models, as demonstrated by the dashed curve in the right hand panel.

particle, $(0 - 1.58) h_{old}$, $(1.58 - 2) h_{old}$ and $(2 - 2.29) h_{old}$. We update h by interpolating over these bins to have 36 neighbours within $2 h_{new}$. We perform the counting during the density summation (to avoid extra computation) for use during the next timestep.

The SPH method involves only pairwise interactions, giving exact momentum and energy conservation. It also relies upon explicit artificial viscosity to model shocks correctly. The artificial viscosity for particle i , contributed by a neighbour j , is a function of $(\vec{v}_i - \vec{v}_j) \cdot (\vec{r}_i - \vec{r}_j)$. This form cannot differentiate between truly converging flows and pure shear flows. Numerical viscosity is thus indiscriminately applied unless a switch is used, such as $|div|/(|div| + |curl| + \epsilon)$ (*e.g.* Steinmetz (1996)). Rather than finding the exact divergence and vorticity to flag particles in strongly convergent (shocking) regions, we use a similar form that is easier to calculate,

$$Switch_i = \frac{\sum_j W_{ij} m_j (\vec{v}_i - \vec{v}_j) \cdot (\vec{r}_i - \vec{r}_j)}{\sum_j W_{ij} m_j |(\vec{v}_i - \vec{v}_j) \cdot (\vec{r}_i - \vec{r}_j)|}$$

A linked-list of particles allocated to a grid of cells is an extremely fast method for locating particle neighbours. Tree structure is an alternative method, though roughly six times slower for uniform densities and very memory intensive. However, with high density contrasts, many particles may accumulate in a few link list cells, rendering the method locally $\mathcal{O}(n^2)$ and thus very slow. We adaptively refine our linked list grid to avoid this problem - to a maximum level of four binary sub-divisions. The storage requirements are naturally much larger but the resulting method slows by only a factor of three in extremely clustered arrangements.

3. The Simulations

The photoionization levels and heating are determined by the background UV flux, in particular the flux at the ionization edge for hydrogen, J_{912} . Observations of the proximity effect hint at little evolution in J_{912} over the range $z = 2$ to 4 (*e.g.* Bechtold (1994)). As shown in the left panel of Figure 1, we apply both a fixed flux (1) and a strongly evolving flux similar to that of Haardt & Madau (1996) lowered to fit the continuum

depression data (2), given by the functional form, $5 \times 10^{-22} ((1+z)/3)^9 \exp(-3(z-2))$. These choices should roughly bracket the true mean UV flux.

The small scale nature of the clouds demands high resolution numerical work, especially as the collisionless nature of the dark matter plus radiative cooling prevent the classical Jean’s length, $k_J^{-1} \approx 0.049(4/(1+z)(T/10^4 K))^{1/2} \Omega_{nr}^{-1/2} h^{-1}$ Mpc from setting a minimum scale. Ω_{nr} refers to density parameter in non-relativistic matter.

We simulate regions of comoving diameter 5.0 Mpc (2.5 h^{-1} Mpc for the CDM model, 3.5 h^{-1} Mpc for the CDM+ Λ model) with $50^3/2$ gas and $50^3/2$ dark matter particles at our highest resolution. We enclose this in a medium resolution buffer of gas and dark matter particles with 8 times the mass, out to 8.0 Mpc and then massive tide particles with 64 times the mass, out to 12.8 Mpc. We apply a linearly evolved external shear to the entire volume, derived from the initial conditions. Thus we make considerable effort to model the long wave, tidal environment well.

We use a sophisticated constrained field code to set up the initial displacements from unperturbed lattice positions, using the Zeldovich approximation. It allows for arbitrary types and numbers of constraints. Our initial conditions finely sample an enormous range of k -space, down to $k = 0.01 h Mpc^{-1}$ for these simulations (see Figure 1 of BW). Periodic simulations must truncate the large scale power beyond the scale of the fundamental mode of the box and the power spectrum is still very flat at $k \sim 1 h Mpc^{-1}$, the scale of Lyman- α simulations.

Most simulations use random regions of the Universe. We prefer to have control parameters which govern some of the major large scale characteristics of the simulation volume. We constrain the density (via ν), bulk flow and tidal fields smoothed over three Gaussian filtered scales R_f , where $\nu = \delta_{L,pk}/\sigma_{R_f}$ the overdensity of the region relative to the *rms* fluctuation level σ_{R_f} . More details and applications of our peak constraint approach are described in BW. For these simulations, we fix ν for $R_f = 0.5$ Mpc and use mean field expectations to set the other parameters, and the values at two other scales, 1.0 and 1.5 Mpc. The ν ’s used are shown in Table 1. Rare events which form large “bright” galaxies by $z \sim 3$ in the patch require higher ν . ν has a Gaussian probability distribution, allowing us to appropriately weight and combine simulations of different ν to create a sample broadly representative of the universe. In creating samples of Lyman- α statistics, the solid angle on the sky subtended and length of spectra generated by the region add further weighting.

Table 1. Initial Conditions used in this work.

Cosmology	Description	ν	e_ν, p_ν^a	Weight ^b	Angle ^c	$\Delta \lambda^c$
CDM	Void	-1.4	0.179, 0.014	0.069	1.47	1.46
	Weak Void	-0.7	0.337, 0.034	0.242	1.26	1.36
	Flat	0.0	0, 0	0.379	1.0	1.0
	Weak Peak	0.7	0.337, 0.034	0.242	0.78	0.77
	Peak	1.4	0.179, 0.014	0.069	0.57	0.62
CDM+ Λ	Flat	0.0	0, 0			

^aTidal (shear) field parameters

^bWeighting due to ν only

^cSolid angle and average length of spectra, $\Delta \lambda$, measured at $z = 3$ relative to Flat region

We describe results for two cosmological models: standard CDM, normalised to $\sigma_8 = 0.67$ with $h = 0.5$, $\Omega_B = 0.05$; COBE-normalised CDM+ Λ , with $h = 0.7$, $\Omega_B = 0.0255$ and $\Omega_{nr} = 0.335$ (shape parameter $\Gamma = 0.225$ and tilt $n_s = 0.94$, which gives a theory in agreement with the shape of the observed large scale power spectrum, see

Figure 1 of BW). We required that $\sigma_{0.5\text{Mpc}} = 1.05$ at $z = 3$ and the number of baryons in the simulation volume to be the same in both models.

4. Results

To analyse our simulations we produce artificial spectra, with signal to noise of 100 and 5 km s^{-1} pixels. We sample a regular spatial grid of lines of sight running along the three axial directions through our simulations. A typical line of sight is $\sim 500\text{ km s}^{-1}$ long and a single simulation sample $\sim 10^6\text{ km s}^{-1}$ at $z=3$. We fit Voigt profiles using an automated profile fitting program, designed to emulate the methods employed by observers. The program identifies each group of lines as a region in the spectrum where the flux drops below 98% of the continuum. χ^2 minimization is used to fit first one line, then two lines and so on. The number of lines that produces the lowest *reduced*- $\chi^2 = \chi^2/d$ is used. d is the number of degrees of freedom remaining for the fit, estimated as 1 per 2 pixels in the line group region minus 3 for each line used in the fit. In practice a line group rarely needs more than 6 lines for a good fit.

Figure 2 demonstrates visually the difference between several runs, as shown in the column depth of neutral hydrogen through the central 2 Mpc of the simulations.

The left panels show the dramatic effect of varying ν and hence the shear field. The filamentary structure is greatly enhanced in even slightly overdense regions. This has important repercussions in the types and numbers of Ly α absorption lines produced, as shown in the bottom left panel of Figure 3. Simulating overdense regions or voids like these is not possible in a periodic box of a similar size, because the density averaged over the box must remain equal to the universal mean value. Even for significantly larger boxes this is a problem.

Comparing the CDM and CDM+ Λ runs (top left and right panels in Figure 2 respectively), it can be seen that the flatter spectrum in the CDM+ Λ case makes the filaments more prominent and the dwarf galaxies less so, but without it having a major impact on the N_{HI} frequency curve. The difference in normalisation is due to the width in redshift of the simulation volume in each cosmology, $dz/dl_{com} = H_0/c(\Omega_{nr}(1+z)^3 + \Omega_\Lambda)^{1/2}$. The high resolution size is $\Delta l_{com}=5\text{ Mpc}$, comoving, in all simulations. Dividing by the ratio of $\Delta z = dz/dl_{com}\Delta l_{com}$ at $z=3$ moves the CDM+ Λ curve down by 0.09 on the top right panel of Figure 3.

The left hand panels of Figure 3 demonstrate that an appropriate fixed choice of $J_{912} = 5 \times 10^{-22}$ can reproduce the observed statistics very well. We have statistically combined 5 CDM simulations to effectively produce a good sample of the universe that includes rarer regions. The advantage of this over a single large simulation is great resolution and importance sampling. The contribution of different regions is apparent. The voids, $\nu < 0$, cause a lowering of the curve, especially at low column depths.

The results of a low resolution run (half that of the standard ones) are shown represented by crosses in the top right panel of Figure 3. Though it underpredicts the low column lines, the high column lines are overpredicted relative to our higher resolution runs: limited resolution mimicks heating by ‘‘puffing’’ up the cores of cold lumps out to greater sizes and thus gives higher cross sections.

In the top right panel of Figure 3 we demonstrate that attempts to renormalise simulations with inappropriate values of the ionizing flux will fail to give the correct frequency of N_{HI} . The curves of interest are the CDM line with a fixed UV history and the scaled low UV points (triangles). These simulations are otherwise identical and have been processed with a fixed value of $J_{912} = 5 \times 10^{-22}$. What *does* scale fairly well is the continuum depression, D_A , shown in the right panel of Figure 1. D_A is defined at the mean value of $1 - \exp(-\tau)$ for a spectral region. This is because the dominant contributors to the optical depth are lines with $N_{HI} \sim 10^{14}$, resulting from barely overdense material for which the UV flux history is less important.

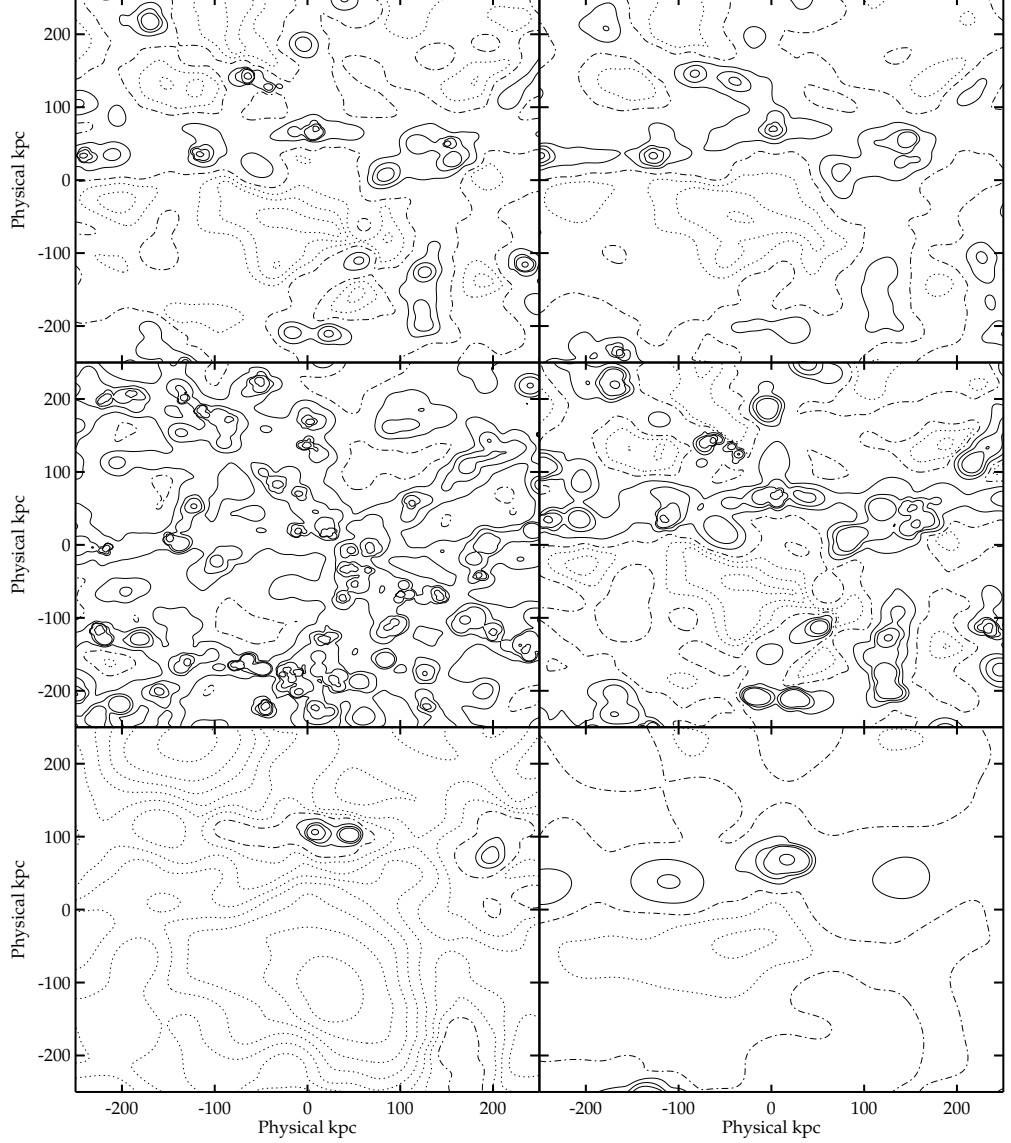


Figure 2. HI Column depth through a cube 2 comoving Mpc thick at $z=3$. The contour levels, in $\log_{10}(\text{cm}^{-2})$, are 11,11.25,11.5,11.75,12,12.25,12.5,12.75,13 (*dotted*), 13.36 (mean density, *dot dashed*) and 14,14.5,15,17 (*solid*). The left panels are CDM simulations, with $\nu = 0, +1.4$ and -1.4 , top to bottom. Note the incredible enhancement of the filamentary structure in the overdense regions. The right hand panels are $\nu = 0$ runs directly comparable with the CDM run in the top left panel. In the top right panel we show a CDM+ Λ run, which has more large scale power and thus more enhanced filaments. The run in the right centre panel had a lower UV flux at early times, resulting in a more clumpy distribution and greatly enhanced HI column depths. The lower right panel shows that poor resolution ($1/2$ the spatial resolution of the upper left panel) will remove much of the structure.

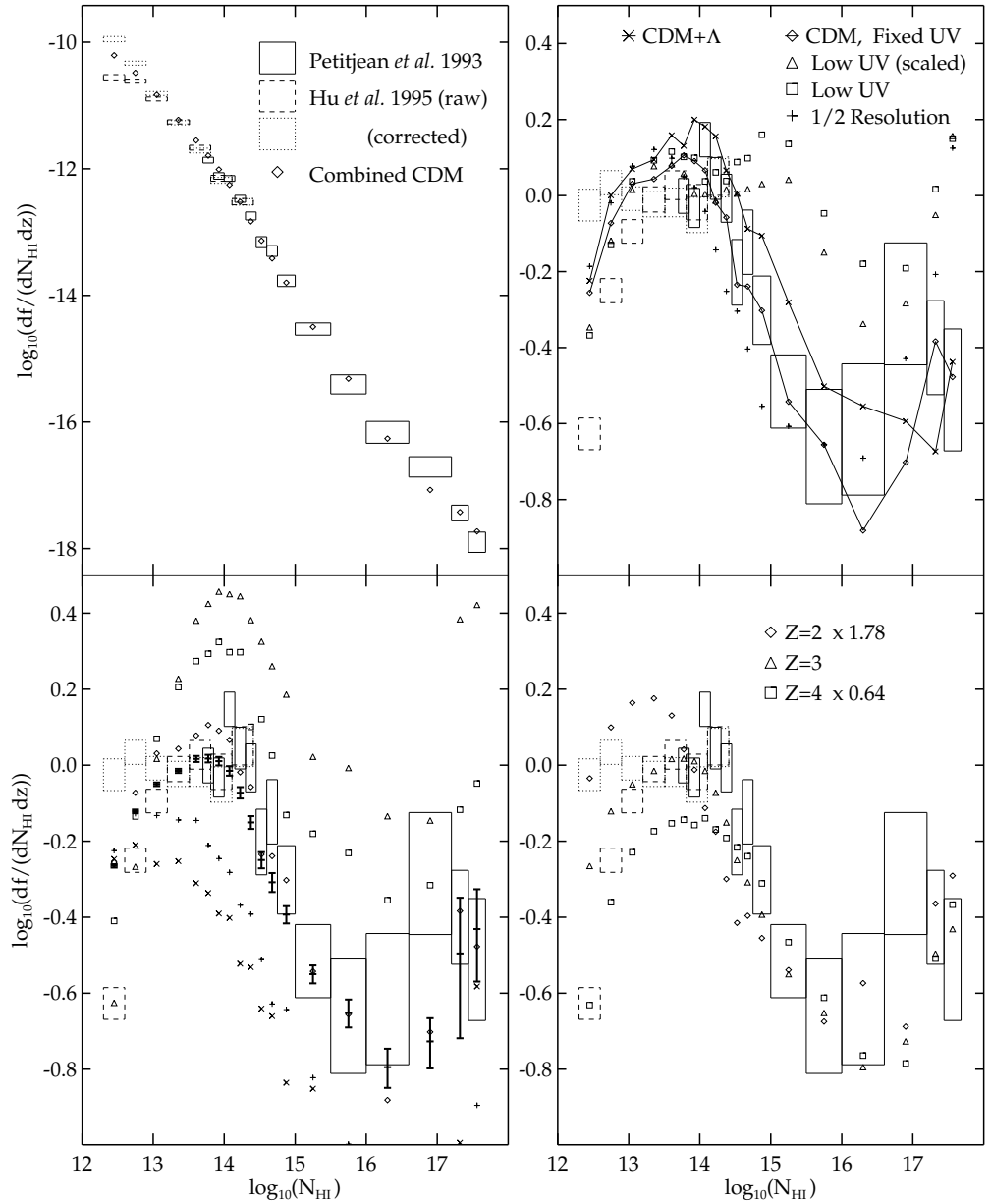


Figure 3. Frequency distribution of lines by N_{HI} . In all frames the boxes represent binned data, box width equalling bin width and the upper and lower edges denoting 1 sigma Poisson errors. At the top left the full range in frequency is plotted and in the remaining graphs, the power law $-1.46 \log_{10}(N_{HI}) + 8.25$ has been subtracted for clarity. On the left, the data from 5 CDM simulations are plotted. The symbols in the lower plot represent (from the top down) the $\nu = 1.4, 0.7, 0, -0.7$ and -1.4 runs respectively and the combined data are shown with 1 sigma Poisson error bars. At the top right, the effects of various choices for the UV flux, numerical resolution and cosmology are compared. The low UV flux at early times results in more clumpiness in the IGM, overproducing lines at intermediate column depths. At the bottom right, the data resulting from combining the CDM simulations are shown at 3 redshifts, divided by $((1+z)/4)^2$. The evolution inferred from the observations is closer to $(1+z)^3$, suggesting a UV flux decreasing with redshift may be needed.

The past history of the UV flux is important for the formation of dense gaseous clumps, as illustrated in the top left and centre right panels of Figure 2; the same UV flux was applied for the post-processing analysis, but the simulation shown in the centre right panel experienced a low UV flux during its evolution (curve (2) in Figure 1). Applying a different flux in post-processing the calculation can of course have no effect on the density distribution and thus cannot compensate for a different history.

Subtracting a power law, derived from the Hu *et al.* (1995) low end slope, from the $f(N_{HI})$ curve of Figure 3 reveals interesting features in the data. If the bumps at $N_{HI} = 10^{14}$ and $N_{HI} = 10^{17}$ (where self shielding of the UV flux starts to become important) are real, they may allow simulations to finely discriminate between parameter choices. The data appear to follow a power law slope of -1.9 in the range $N_{HI} = 10^{14} - 10^{16} \text{ cm}^{-2}$, which our runs with fixed flux reproduce and those with low UV flux at early times do not. This is also apparent in the results of Rauch *et al.* (1996) who apply a UV flux that slowly increases with redshift. Simulations that calculate the UV flux history (Miralda-Escudé *et al.* (1996), Mückel *et al.* (1996)) perform fairly well, suggesting that a more detailed self-consistent treatment could produce a strong result. The excess of intermediate column lines seen for the low UV simulations may be due to unrealistically low energy input at early times; specifically there should be input from early stars. We are testing this hypothesis using a UV flux history similar to curve (3) in Figure 1. Star formation and supernova feedback would also inhibit the formation of the extremely dense, cool clumps associated with this excess. We are now incorporating these processes using a general chemical evolution code.

We have illustrated that the Lyman alpha forest is a sensitive probe of the conditions that operated at $z \sim 5$ to 2. It is clear that we must produce a comprehensive sample if we are to deliver reliable predictions to the observers of the clouds. Finding forest observables that allow us to separate the influence of primordial power spectrum shape and amplitude, cosmological parameters such as Ω_{Λ} , Ω_{cdm} , Ω_{hdm} , H_0 and Ω_B , the ionization history and local energy injection from galaxies (feedback) will be a challenge to the growing group of cloud simulators, in close collaboration with the observers of the forest. Nonetheless it is clear that the basic model (whether CDM or CDM+ Λ) with $\sigma_{0.5 \text{ Mpc}} \sim 1$ at $z \sim 3$ provides a rather good fit to the data.

Acknowledgments. Support from the Canadian Institute for Advanced Research and NSERC is gratefully acknowledged. We would like to thank John Lattanzio and Joe Monaghan, who were involved in the early phases of this project, using an SPH-Multigrid code of earlier vintage.

References

- Bechtold, J. 1994, in *QSO Absorption Lines*, ESO Astrophysics Symposia, G. Meylan (ed), Springer-Verlag, p.299
- Bond, J.R. & Wadsley, J.W. 1996, to be published in *Computational Astrophysics*, 12th Kingston Meeting on Theoretical Astrophysics, *in preparation*, (BW)
- Davé, R., Hernquist, L., Weinberg, D. & Katz, N. 1996, Accepted by ApJ
- Haardt, F. & Madau, P. 1996, ApJ, 461, 20
- Hernquist, L., Katz, N., Weinberg, D. & Miralda-Escudé, J. 1996, ApJ, 457, L51
- Hu, E.M., Kim, T.S., Cowie, L.L., Songaila A. & Rauch, M. 1995, ApJ, 466, 46
- Miralda-Escudé, J., Cen, R., Ostriker, J.P. & Rauch, M. 1996, ApJ, 471, 582
- Monaghan, J.J. 1992, ARA&A, 30, 543
- Mückel, J.P., Petitjean, P., Kates, R.E. & Riediger, R., 1996 \hat{a} , 308, 17

- Petitjean, P., Webb, J.K., Rauch, M., Carswell, R.F. & Lanzetta, K. 1993, MNRAS, 262, 499
- Rauch, M., Haehnelt, M.G. & Steinmetz, M. 1996, Submitted to ApJ
- Steinmetz, M. 1996, to be published in *The Early Universe with the VLT*, ESO Workshop
- Zhang, Y., Anninos, P., Norman, M.L. & Meiksin, A. 1996, submitted to ApJ